Short cracks and V-notches: Finite Fracture Mechanics vs. Cohesive Crack Model

P. Cornetti *, A. Sapora, A. Carpinteri

Department of Structural, Building and Geotechnical Engineering, Politecnico di Torino, Corso Duca degli Abruzzi 24, 10129 Torino, Italy

ABSTRACT

In recent years, Finite Fracture Mechanics has proven to be an effective tool to estimate the strength of mechanical components, allowing fast strength predictions suitable for preliminary sizing and optimization of structures. In the present paper, we intend to corroborate the Finite Fracture Mechanics approach by showing that failure load estimates are very close to the ones provided by the well-established Cohesive Crack Model. To this aim, we consider two classical fracture mechanics problems, i.e. short cracks and V-notches. In the latter case, we believe to be of relevance also the Cohesive Crack Model semi-analytical solution herein provided.

© 2016 Elsevier Ltd. All rights reserved.

1. Introduction

The Cohesive Crack Model (CCM) allows one to get accurate and physically-based strength predictions in plain or composite structural elements with stress concentrations or stress intensifications. Unfortunately, CCM usually requires a numerical implementation with large computing times that are not acceptable for preliminary sizing of structural details.

On the other hand, fast strength predictions can be obtained by applying the point stress criterion (or the average stress criterion). These methods predict failure when the stress at (or over) a certain distance (the so-called critical distance) reaches the material tensile strength. Nevertheless these approaches do not possess a clear physical background and show some drawbacks [1]; moreover, they require expensive experimental programs to identify the critical distances for different materials and geometries [2]. On the other hand, the recently introduced Finite Fracture Mechanics (FFM) allows one to overcome this shortcoming since the length of the critical distance is an outcome of the structural problem [1,3,4]. Furthermore FFM possesses a clear physical interpretation, i.e. fracture is supposed to propagate by finite steps. Thus, in the authors' opinion, FFM can be seen as the right candidate criterion to achieve accurate, physically-based and fast strength predictions.

Aim of the present paper is to corroborate this choice by showing that, for a couple of simple, yet relevant, case studies, the CCM and FFM strength predictions are in a very good agreement with each other. The two geometries to be investigated are represented by an infinite slab containing (i) a short crack and (ii) a (deep) re-entrant corner, both under simple mode I loading conditions. As well known, in both cases the Linear Elastic Fracture Mechanics (LEFM) fails in predicting the failure load. On the other hand, we will see that CCM and FFM correctly describe the transition from a toughness-governed failure to a strength-governed one, as the crack length decreases in the former case, and as the notch opening angle increases in the latter case. Noteworthy, both problems are solved in an almost completely analytical fashion.

---

* Corresponding author. Tel.: +39 0110904901; fax: +39 0110904899.
  E-mail address: pietro.cornetti@polito.it (P. Cornetti).

Nomenclature

(x,y)	spatial coordinates
F	concentrated force
σ_y	normal stress in y direction
σ_c	material tensile strength
σ	remote uniaxial stress
σ_f	remote failure stress
E'	Young modulus in plane strain conditions
$\mathcal{G}$	strain energy release rate
$\mathcal{G}_c$	fracture energy
a	crack length
a_p	process zone size
a_{pc}	process zone size at incipient failure
l_{ch}	Irwin length
Δ	crack increment
Δ_c	finite crack advancement
w	crack opening displacement
w_c	critical displacement
K_I	Mode I stress intensity factor
K_{Ic}	fracture toughness
K_I^*	generalized stress intensity factor
K_{Ic}^*	generalized fracture toughness
ω	notch opening angle
α	$\pi - \omega/2$, angle
λ	William's eigenvalue
$\gamma(\omega), \beta(\omega), \mu(\omega)$	shape functions
ξ	dimensionless generalized fracture toughness

Before starting to investigate the two geometries, it is worth observing that the agreement between CCM and FFM is to be expected, despite the different – continuous vs. discrete – crack growth mechanism, because they are both based on the same energy balance. The energy spent to create the new (unit) fracture surface is in fact $\mathcal{G}_c$ for both models (whereas the theory of critical distances usually does not fulfill this energy balance). A similar analogy between CCM and FFM holds also for the stress requirement: as well as the choice of the cohesive law is free for CCM, analogously the stress requirement to be coupled with the energy balance in FFM can be chosen arbitrarily (i.e. according to the material at hand). Moreover, once we fix the fracture energy and the tensile strength, the effect of the cohesive law shape as well as of the stress requirement expression is relatively weak for process zones/crack extensions much smaller than other geometrical lengths (see e.g. [5] for what concerns CCM).

Wishing to compare CCM and FFM, we expect similar predictions by CCM with a constant cohesive law and by the FFM approach with a point-wise stress requirement – as proposed by Leguillon [3]. Analogously, similar predictions are argued for CCM with a linearly descending cohesive law and for the FFM approach with an average stress condition – as proposed by Cornetti et al. [1] and applied to V-notches in [6]. In fact, the former choices provides a smaller process zone/crack extension but with a higher stress field, whereas the latter features yield a larger process zone/crack extension but with a lower stress field. This conjecture is confirmed for the pull–push shear test [7].
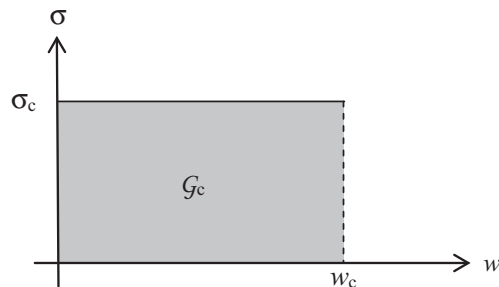

Fig. 1. Dugdale cohesive law.

Aiming to achieve analytical results, herein we will consider the first pair of models, i.e. Dugdale model for CCM, and Leguillon's version of FFM.

Dugdale model prescribes a constant stress over the process zone, see Fig. 1. It means that the structure behaves elastically whenever the stress is lower than the tensile strength σ_c. When, increasing the load, at a given point the tensile strength is reached, there a fictitious crack occurs, i.e. the crack lips open but the interaction between the crack faces does not vanish. The stress remains constant and equal to σ_c as the crack opening w grows from 0 to the threshold value w_c. As w exceeds w_c, the interactions (i.e. the stress) between crack faces suddenly drop to zero and a real crack takes place. Consequently, the fracture energy $\mathcal{G}_c$ is given by the product of σ_c times w_c, represented by the grey area in Fig. 1. It is worth noting that the computation of the maximum load is relatively simple for the Dugdale cohesive law: the highest load value is achieved when the opening displacement first reaches the threshold value w_c (provided that the geometry is positive, i.e. the Stress Intensity factor (SIF) is monotonically increasing with the crack length). For different cohesive law shapes it is achieved earlier, i.e. before the appearance of the real crack; thus its computation has to be pursued numerically (or at least in part, see e.g. [8]) even for very simple geometries.

Leguillon's FFM approach states that a crack appears or propagates by Δ whenever the normal stress over the crack increment Δ (here the crack is supposed to propagate along the x-axis) is larger than the material tensile strength σ_c and, contemporaneously, the energy available for the finite crack increment is larger than $\mathcal{G}_c \times \Delta$:

$$\begin{cases} \sigma_y(x) \geqslant \sigma_c, & a \leqslant x \leqslant a + \Delta \\ \int_a^{a+\Delta} \mathcal{G}(a')\mathrm{d}a' \geqslant \mathcal{G}_c\Delta \end{cases} \tag{1}$$

where a is the initial crack length (or semi-length for symmetrical geometries, as in Fig. 2) and $\mathcal{G}$ is the strain energy release rate. The failure load is the lowest load value for which both inequalities in Eq. (1) are satisfied. Usually the stress field ahead the crack tip (or ahead the point where the new crack appears) is decreasing, whereas the strain energy release rate is monotonically increasing with the crack length a'. In this case (i.e. a positive geometry, which is by far the most common situation and, specifically, the case considered in this paper), the failure load is achieved when the two inequalities are strictly verified. Thus Eq. (1) reverts to a system of two equations in two unknowns, the crack advancement Δ_c and the failure load, implicitly embedded in the strain energy release rate $\mathcal{G}$ and in the stress field σ_y. Recalling Irwin relationship between the strain energy release rate $\mathcal{G}$ and the SIF K_I (and between the fracture energy and the fracture toughness), we can cast Eq. (1) as:

$$\begin{cases} \sigma_y(x) = \sigma_c, & a \leqslant x \leqslant a + \Delta \\ \int_a^{a+\Delta} K_I^2(a')\mathrm{d}a' = K_{\mathrm{Ic}}^2\Delta \end{cases} \tag{2}$$

In the following, we will make use also of the so-called characteristic (Irwin) length l_{ch}, defined as $(K_{\mathrm{Ic}}/\sigma_c)^2$.

Eventually, we want to highlight that the FFM analytical solution for the short crack geometry and the CCM semi-analytical solution for the V-notch provided in this paper are original. On the other hand, the CCM solution for the Griffith crack (see, e.g., [9]) and the FFM solution for the V-notch [3,10] are already available in the Scientific Literature.

2. Short cracks

The first case we are considering is an infinite slab with a central crack of length $2a$ under a remote uni-axial stress σ orthogonal to the crack (i.e. the Griffith crack, see Fig. 2a). A completely analytical solution for both fracture criteria is achievable for this simple geometry.

2.1. Cohesive Crack Model

The original Dugdale [11] work aimed to get an estimate of the plastic zone ahead of a crack in sheets under a sufficiently small remote tensile stress, which is equal to the well-known value $(\pi/8) \times l_{\mathrm{ch}}$ at incipient failure. However, an exact value of the process zone size can be obtained analytically also when the remote stress approaches the limit stress σ_c, i.e. for short cracks. The procedure to get these values is briefly sketched below. Details can be found, e.g., in [9]. It is worth observing that the only datum needed is the SIF for a pair of normal forces acting at a generic point of the crack faces. Such a result is known exactly and its expression can be found in [12].

According to CCM, the length of the process zone a_p is such to eliminate the stress singularity at the fictitious crack tip, i.e. at $x = a + a_p$ (see Fig. 2b). The SIFs due to the remote stress σ and to the cohesive stresses σ_c acting in the process zone ($a < x < a + a_p$) read, respectively:

$$K_I(\sigma) = \sigma\sqrt{\pi(a + a_p)} \tag{3a}$$

$$-K_I(\sigma_c) = 2\sigma_c\sqrt{\frac{a + a_p}{\pi}}\arccos\frac{a}{a + a_p} \tag{3b}$$

Hence, the condition of null SIF yields the length of the process zone as a function of the stress level σ as:
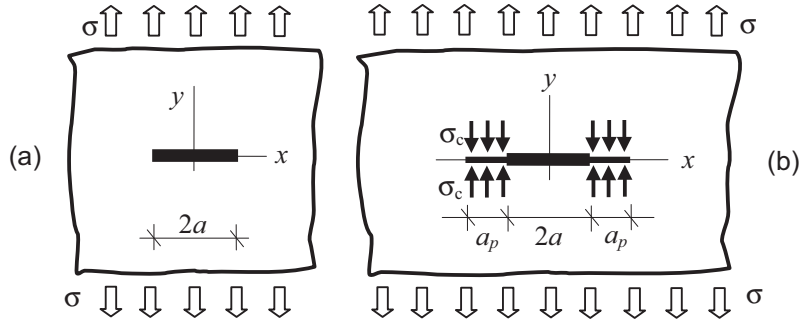
Fig. 2. A central through crack in an infinite slab with a uniformly applied remote stress σ orthogonally to the crack (Griffith crack, a) and details of the process (or plastic) zone size ahead the crack tip (b) according to Dugdale model.

$$\frac{a_p}{a} = \sec\left(\frac{\pi\sigma}{2\sigma_c}\right) - 1 \tag{4}$$

Starting from the SIF for a pair of normal forces acting at a generic point of the crack faces, it is also possible, by Paris' equation [12], to achieve the crack opening displacement function $w(x)$. It is given by an integral made up of three terms, the first one related to the external remote stress and the second and third terms to the two symmetric cohesive zones at the crack edges. The integral can be solved analytically, yielding ($a \leqslant x \leqslant a + a_p$):

$$w(x) = \frac{4\sigma_c}{\pi E'}\left[(x+a)\text{arccosh}\frac{(a+a_p)^2 + ax}{(a+a_p)(x+a)} - (x-a)\text{arccosh}\frac{(a+a_p)^2 - ax}{(a+a_p)(x-a)}\right] \tag{5}$$

Thus the displacement at the real crack tip ($x = a$), i.e. the crack tip opening displacement (CTOD) is:

$$w(a) = \frac{8\sigma_c a}{\pi E'}\ln\left(\frac{a+a_p}{a}\right) \tag{6}$$

where E' is the Young modulus in plane strain condition. The maximum achievable remote stress σ_f is reached when the CTOD attains its threshold value w_c. This condition, together with $\mathcal{G}_c = \sigma_c\, w_c = K_{\text{Ic}}^2/E'$, leads to:

$$a_{\text{pc}} = a\left(e^{\frac{\pi l_{\text{ch}}}{8a}} - 1\right) \tag{7}$$

which provides (see e.g. [9]) the process zone size at incipient failure (i.e. when the real crack starts growing). Upon substitution of Eq. (7) into (4), we finally achieve the corresponding failure stress σ_f:

$$\frac{\sigma_f}{\sigma_c} = \frac{2}{\pi}\arccos\left(e^{-\frac{\pi l_{\text{ch}}}{8a}}\right) \tag{8}$$

Eqs. (7) and (8) are plotted in Fig. 3a and b, respectively. Furthermore, note that, for sufficiently large cracks (i.e. $a/l_{\text{ch}} \to \infty$), Eqs. (7) and (8) provide Dugdale plastic zone size estimate ($\pi/8) \times l_{\text{ch}}$ and the LEFM failure stress $K_{\text{Ic}}/\sqrt{\pi a}$, respectively. On the other hand, the process zone tends to infinite and the failure stress to σ_c for very short cracks, i.e. if $a/l_{\text{ch}} \to 0$ (see Fig. 3). It is clear that the concept of "short" or "large" crack has not to be intended absolutely, but with respect to the material length l_{ch}.

2.2. Finite Fracture Mechanics

To apply FFM criterion, we need the stress field ahead the crack tip (Westergaard solution) as well as the SIF (Fig. 2a). They read, respectively ($x > a$):

$$\sigma_y(x) = \frac{x}{\sqrt{x^2 - a^2}}\sigma \tag{9a}$$

$$K_I(a) = \sigma\sqrt{\pi a} \tag{9b}$$

Upon substitution of Eq. (9) into the FFM system (2) and by integration, we get:

$$\begin{cases} \left(\frac{\sigma}{\sigma_c}\right)^2 = 1 - \left(\frac{a}{a+\Delta}\right)^2 \\ \left(\frac{\sigma}{\sigma_c}\right)^2 = \frac{2/\pi\ l_{\text{ch}}}{2a+\Delta} \end{cases} \tag{10}$$
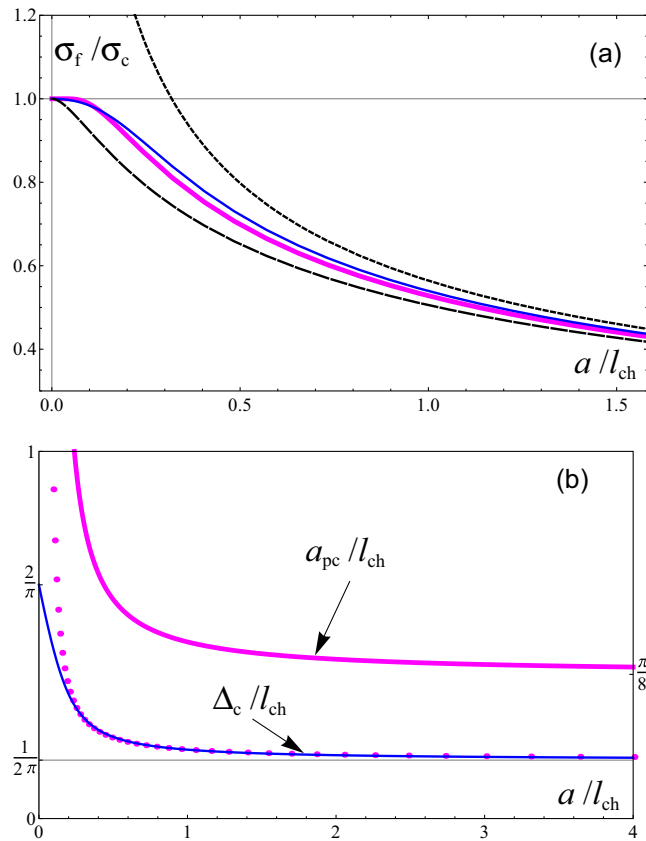
Fig. 3. Normalized failure stress vs. normalized crack length (a): FFM (thin line), CCM (thick line), PM (dashed line), LEFM (dotted line). Normalized crack advancement (FFM, thin line), process zone size (CCM, thick line), CCM crack length for $\psi = 0.35$ (dots) vs. normalized crack length (b).

The solution of the system provides the finite crack extension Δ_c as the solution of the following cubic equation:

$$\Delta_c(2a + \Delta_c)^2 = \frac{2}{\pi} l_{ch}(a + \Delta_c)^2 \tag{11}$$

Eq. (11) has only one positive, real solution, which can be expressed analytically (see Appendix A). Once Δ_c is obtained, the failure stress σ_f is obtained by substitution of Δ_c into either the first or the second equation of the system (10). Taking the first one, we get:

$$\frac{\sigma_f}{\sigma_c} = \frac{\sqrt{\Delta_c(2a + \Delta_c)}}{a + \Delta_c} \tag{12}$$

The normalized failure stress given by Eq. (12) and the finite crack extension provided by Eq. (11) are plotted in Fig. 3a and b, respectively. Numerical values are provided in Table 1 as a function of the normalized crack length a/l_{ch}. It is evident the excellent agreement between the failure stress estimates provided by the FFM approach and CCM, the relative

Table 1
Griffith crack: normalized failure stress vs. crack length according to different criteria. Percentage error with respect to CCM prediction.

a/l_{ch}	Normalized failure stress (σ_f/σ_c)				% error with respect to CCM		
	CCM	FFM	PM	LEFM	FFM	PM	LEFM
0	1	1	1	∞	0	0	∞
0.1	0.987	0.984	0.922	1.784	−0.37	−6.57	+80.7
0.2	0.910	0.928	0.831	1.262	+1.99	−8.76	+38.6
0.5	0.699	0.722	0.652	0.799	+3.30	−6.72	+14.2
1	0.528	0.539	0.506	0.564	+2.15	−4.23	+6.84
2	0.386	0.391	0.377	0.399	+1.19	−2.39	+3.35
10	0.177	0.178	0.176	0.178	+0.25	−0.53	+0.66

error being always less than 3.5%. In Fig. 3a and Table 1 we provided also the failure stress predictions given by LEFM and the point stress method (PM). As well known, LEFM provides an infinite failure load for vanishing cracks, a result that is physically inconsistent. On the other hand, the PM predictions, that are obtained setting $\varDelta_c = (1/2\pi) \times l_{ch}$ in Eq. (12), fulfill the limit cases as CCM and FFM do, i.e. $\sigma = \sigma_c$ for $a = 0$ (with flat tangent) and the LEFM estimate for $a \rightarrow \infty$. However, predictions based on simple PM are relatively far from the CCM ones, the maximum error reaching 9%. Moreover, note that while LEFM provides always an overestimation of the failure load with respect to the CCM estimate, PM always underestimates this value.

In Fig. 3b we plotted the process zone size (at incipient failure) and the finite crack advancement vs. the crack length. It is worth noting that, although the absolute values of the two lengths are pretty far from each other, the trend with respect to the normalized crack length is almost identical. The finite crack advance $\varDelta_c$ decreases monotonically from the value $(2/\pi) \times l_{ch}$, i.e. the critical distance for the so called line-energy (LE) approach for central cracks [13], to the limit value $(1/2\pi) \times l_{ch}$, i.e. the critical distance according to PM.

The large difference in absolute values between the process zone in the CCM and the finite crack extension in FFM may be explained observing that, while the finite crack extension is a "true" crack (no stresses among the new crack lips), the process zone is a fictitious crack, since cohesive stresses are present. Thus, maybe, it is more correct to compare the finite crack advancement with the portion of the process zone with $w > w_c$, i.e. when the crack is stress free. Nevertheless, this portion is null. However, an infinite number of intermediate alternatives can be proposed defining the crack length in the CCM as the zone where the crack opening is larger than a fraction $0 < \psi < 1$ of the critical displacement w_c. This can be easily done by imposing the right hand side of Eq. (5) equal to $(\psi \times w_c)$ and solving the consequent equation with respect to x, now representing the crack length in the CCM. As shown in Fig. 3b a very good agreement between the crack lengths provided by the two models is obtained for $\psi \cong 0.35$, i.e. considering the "true" crack in the CCM when the crack opening is larger than (about) one third of the critical displacement. It must be observed however that for vanishing cracks the behavior still remains different, since the CCM crack length diverges for any $\psi \neq 0$.

3. Re-entrant corner

Let us now consider a V-notched structure under mode I loading conditions (Fig. 4a), ω being the notch opening angle $(0 < \omega < \pi)$. Since Williams' work, we know that the stress field is singular, the asymptotic stress field ahead the notch tip being (along the notch bisector):

$$\sigma_y = \frac{K_I^*}{(2\pi x)^{1-\lambda}} \tag{13}$$

The order of singularity is $(1 - \lambda)$, where the eigenvalue λ is comprised between 0.5, for $\omega = 0$, and 1, for $\omega = \pi$, when the singularity disappears (straight edge). K_I^* is the Generalized (or Notch) Stress Intensity Factor (GSIF) and univocally characterizes the asymptotic stress field. Eq. (13) shows that, except for the extreme cases, the stress field is singular, but with a power of the singularity less than 1/2. Therefore, both simple stress criteria (i.e. $\sigma < \sigma_c$ in any point of the structure) and LEFM fail in predicting the strength of V-notched components, providing respectively null or infinite failure loads.
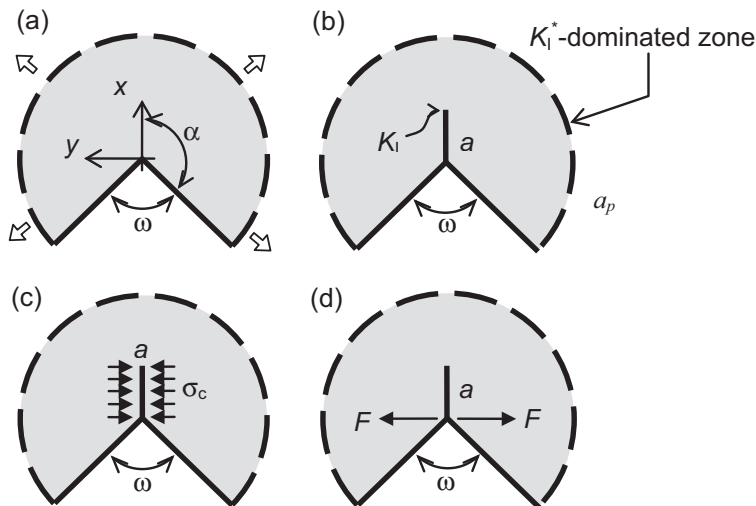

Fig. 4. Re-entrant corner under mode I loading: reference system (a); V-notch emanated crack (b); V-notch emanated-crack loaded by a constant stress field (c); V-notch emanated crack loaded by a pair of opening forces at the V-notch tip (d).

In his pioneering paper, Carpinteri [14] proposed to correlate the failure load with the critical value of K_I^*, i.e. the generalized fracture toughness K_{Ic}^*. In the following, we will show that both CCM and FFM corroborate this conjecture, furthermore providing an expression relating the generalized fracture toughness to the tensile strength and the fracture toughness.

We finally observe that the Dugdale model provides a rough estimate of the plastic zone ahead a V-notch. For a further insight of the plastic zone ahead a V-notch, the reader is referred to the papers by Hills and Dini [15] and Flicek et al. [16].

3.1. Cohesive Crack Model

The V-notch problem (under mode I loadings) has been faced by means of CCM with a rectangular cohesive law (Dugdale model) by several authors. Gomez and Elices [17] addressed the problem numerically, i.e. by implementing CCM in a Finite Element code. This approach allows the Authors to consider both sharp/blunt and deep/shallow V-notches. Restricting the analysis to sharp and deep V-notches, i.e. with zero root radius and a notch depth much larger than l_{ch} (see Fig. 4a), Henninger et al. [18] – through an asymptotic matching approach – and Shi [19] – using suitable path-independent integrals and some simplifying assumptions – provided semi analytical solutions. However, we will show that it is also possible to achieve the solution by simply exploiting suitable shape functions, some approximate and some exact, available in the Scientific Literature.

Let us consider the SIF of a crack stemming from a V-notch tip (Fig. 4b) falling within the K_I^*-dominated zone. In the most general case, it depends on the crack length a, the notch-opening angle ω and the GSIF K_I^*; thus, formally, we can write:

$$K_I = f(a, \omega, K_I^*) \tag{14}$$

Taking as fundamental quantities a and K_I^*, we can apply Buckingham's Π theorem of dimensional analysis, which yields:

$$K_I = \mu(\omega) K_I^* a^{\lambda-1/2} \tag{15}$$

At the Authors' best knowledge, Eq. (15) dates back to Hasebe and Iida [20]. More recently, Philipps et al. [21] and Livieri and Tovo [22] provided very accurate μ values; the former ones are reported in Table 2. Furthermore, an approximate function for μ was deduced analytically by Savruk and Rytsar [23] (see also [24]). Its expression is reported in Appendix B; differences with respect to the values given in [21] are less than 1%. In the following, plots make use of the approximate function, whereas tables exploit the numerical values provided in [21].

According to Dugdale model, a process zone appears ahead the V-notch vertex for any non-zero load level. In the process zone, the stress is constant and equal to the critical stress σ_c (see Fig. 4c). Such a uniform stress distribution generates a SIF equal to:

$$K_I = -\gamma(\omega) \sigma_c \sqrt{a} \tag{16}$$

The shape function $\gamma(\omega)$ is provided in [12] with an accuracy better than 1%. It is reported in Appendix B and numerical values are presented in Table 2. The length a_p of the process zone is thus determined by the condition of a vanishing SIF at the crack tip, i.e.:

$$\mu(\omega) K_I^* a_p^{\lambda-1/2} - \gamma(\omega) \sigma_c \sqrt{a_p} = 0 \tag{17}$$

leading to:

$$a_p = \left(\frac{\mu K_I^*}{\gamma \sigma_c}\right)^{\frac{1}{1-\lambda}} \tag{18}$$

It is worth observing that Eq. (18) contains, as limit cases, $a_p = (\pi/8) \times (K_I/\sigma_c)^2$ for $\omega = 0$, i.e. a (large) crack (thus coinciding with Eq. (4) for low applied stresses), and $a_p = (\sigma/\sigma_c)^\infty$ for a flat edge ($\omega = \pi$), σ being the tensile stress along the edge. This last expression is coherent, providing a null process zone for $\sigma < \sigma_c$ and an infinite one for $\sigma > \sigma_c$.

Table 2
Re-entrant corner: eigenvalues, shape factors and normalized generalized fracture toughness according to different criteria vs. notch-opening angle. Percentage error with respect to CCM prediction.

ω	λ	μ	γ	β	ξ_{CCM}	ξ_{FFM}	ξ_{PM}	% error with respect to CCM	
								FFM	PM
0	1/2	1	$2\sqrt{2/\pi}$	$\sqrt{2/\pi}$	1	1	1	0	0
$\pi/6$	0.5015	1.005	1.600	0.800	0.999	0.999	1	−0.03	+0.05
$\pi/3$	0.5122	1.017	1.619	0.813	1.016	1.017	1	+0.09	−1.62
$\pi/2$	0.5445	1.059	1.656	0.857	1.055	1.063	1	+0.80	−5.17
$2/3\pi$	0.6157	1.161	1.720	0.956	1.124	1.137	1	+1.21	−11.02
$5/6\pi$	0.7520	1.394	1.822	1.142	1.208	1.181	1	−2.29	−17.24
π	1	$1.1215\sqrt{\pi}$	$1.1215\sqrt{\pi}$	$\sqrt{\frac{4\pi}{\pi^2-4}}$	1	1	1	0	0

As the external load increases, K_I^* grows proportionally. According to Eq. (18), also the process zone will increase, with a power law of the load equal or larger than 2. According to the CCM terminology, the fictitious crack tip is placed at the distance a_p from the V-notch vertex; the real crack does not appear as far as the CTOD, i.e. the opening displacement at the V-notch tip, is smaller than the threshold value w_c. We can easily compute the CTOD starting from the SIF for a pair of forces F (see Fig. 4d) acting at the V-notch tip. For this geometry, the solution is available in closed form [25] as:

$$K_I = \beta(\omega)\frac{F}{\sqrt{a}} \tag{19}$$

The explicit expression of $\beta(\omega)$ is given in Appendix B. Hence, a straightforward application of Castigliano's theorem (Paris' equation) allows one to compute the CTOD as:

$$w = \frac{2}{E'}\int_0^{a_p}\left[K_I(K_I^*,a) + K_I(\sigma_c,a)\right]\frac{\partial K_I(F,a)}{\partial F}da \tag{20}$$

Upon substitution of Eqs. (15), (16) and (19) into Eq. (20), and exploiting Eq. (18) we get:

$$w = \frac{2\beta\gamma(1-\lambda)}{\lambda}\frac{\sigma_c}{E'}\left[\frac{\mu K_I^*}{\gamma\sigma_c}\right]^{\frac{1}{1-\lambda}} \tag{21}$$

The real crack tip will appear at the V-notch vertex only when the CTOD reaches its critical value w_c: the interaction between the crack lips vanishes and the structure reaches the maximum sustainable load. The condition $w = w_c = K_{Ic}^2/(E'\sigma_c)$ applied to Eq. (21) provides the generalized fracture toughness according to CCM:

$$K_{Ic}^* = \xi_{CCM}(\omega)\sigma_c l_{ch}^{1-\lambda} \tag{22}$$

where the dimensionless coefficient ξ_{CCM} is given by:

$$\xi_{CCM}(\omega) = \frac{\gamma}{\mu}\left[\frac{\lambda}{2\beta\gamma(1-\lambda)}\right]^{1-\lambda} \tag{23}$$

and represents the dimensionless fracture toughness according to CCM. By means of Eq. (22), CCM proves that the GSIF can be effectively used to correlate failure of V-notched components as argued by Carpinteri [14]. Furthermore, Eq. (22) shows the dependence of the generalized fracture toughness on the tensile strength and the fracture toughness. It is easy to check that ξ_{CCM} is equal to unity for $\omega = 0,\pi$, so that, as expected, the generalized fracture toughness equals the fracture toughness and the tensile strength for a crack and a flat edge, respectively. The dependence of the parameter ξ_{CCM} on the notch-opening angle ω is drawn in Fig. 5a and numerical values are given in Table 2.

On the other hand, substitution of Eq. (22) into Eq. (18) provides the expression for the process zone length a_{pc} at critical conditions:

$$a_{pc} = \frac{\lambda}{2\beta\gamma(1-\lambda)}\;l_{ch} \tag{24}$$

which varies from the well-known Dugdale plastic zone estimate $(\pi/8)\times l_{ch}$ for a crack to infinite for a flat edge (see Fig. 5b). The extreme values are the same encountered in Section 2, for an infinite and a vanishing crack length, respectively. To investigate further this analogy, in Fig. 6a we plot the normalized lengths of the process zone ahead a short crack (Eq. (7)) vs. twice the arctangent of (l_{ch}/a) and ahead a V-notch (Eq. (24)) vs. the notch opening angle ω. The fair agreement between the two curves means that the process zone length ahead a crack of length a is approximately equal to the one ahead a (deep) V-notch with opening angle $\omega = 2\arctan(l_{ch}/a)$, see Fig. 6b.

3.2. Finite Fracture Mechanics

By the asymptotic matching technique, Leguillon [3] provided the FFM solution for the re-entrant corner problem. Here we provide the solution exploiting the shape functions introduced in the previous section. To apply the FFM criterion, we simply need to substitute Eqs. (13) and (15) into Eq. (2):

$$\begin{cases} \frac{K_I^*}{(2\pi\varDelta)^{1-\lambda}} = \sigma_c \\ \left(\mu K_I^*\varDelta^\lambda\right)^2 = 2\lambda K_{Ic}^2\varDelta \end{cases} \tag{25}$$

The solution of such a system yields the value of the finite crack advance $\varDelta_c$, as well as the generalized fracture toughness K_{Ic}^*:

$$\varDelta_c = \frac{2\lambda}{\mu^2(2\pi)^{2(1-\lambda)}}l_{ch} \tag{26a}$$

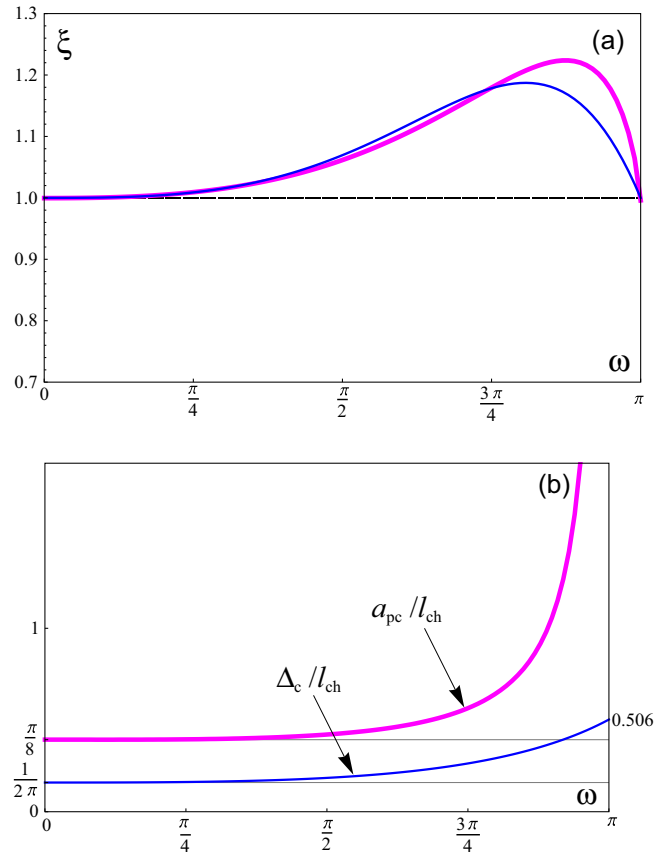$$K_{Ic}^* = \xi_{FFM}(\omega)\sigma_c\;l_{ch}^{1-\lambda} \tag{26b}$$

Fig. 5. Normalized generalized fracture toughness ξ vs. notch-opening angle ω according to different fracture criteria (a): FFM (thin line), CCM (thick line), PM (dashed line). Normalized crack advancement (FFM, thin line) and process zone size (CCM, thick line) vs. notch-opening angle (b).
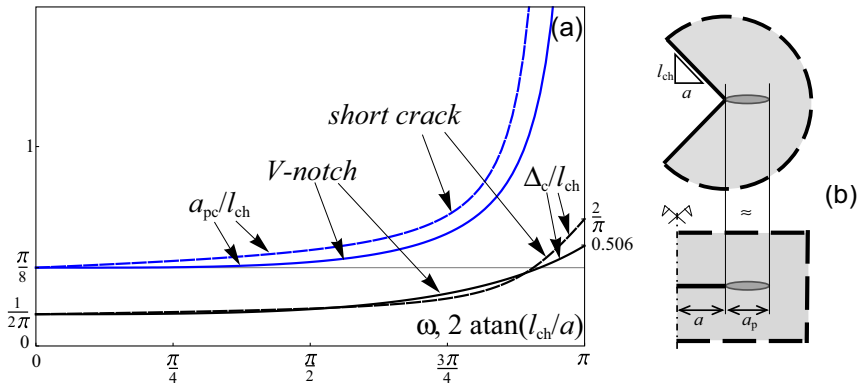

Fig. 6. Analogy between the sizes of the cohesive process zone (upper pair) and of the crack increment (lower pair) ahead a short crack (dashed lines) and a deep V-notch (continuous lines): plots (a) and geometrical sketch (b).

The dimensionless coefficient ξ_{FFM} (i.e. the dimensionless fracture toughness according to FFM) is now given by [10]:

$$\xi_{FFM}(\omega) = \left[\frac{2\lambda(2\pi)^{2\lambda-1}}{\mu^2}\right]^{1-\lambda} \tag{27}$$

which is plotted in Fig. 5a and tabled in Table 2, together with the CCM and PM estimates. PM result is obtained by setting $\Delta = \Delta_c = (1/2\pi) \times l_{ch}$ in the first equation of the system (25); hence ξ_{PM} is constant and equal to unity for any notch opening angle. Once more, Fig. 5 and Table 2 show the excellent agreement between the FFM and CCM approaches: the two

predictions are almost coincident, some discrepancies rising only in the range 150–180°. The relative errors in Table 2 are always less than 2.3%. On the other hand, predictions based on the simple PM are relatively far from the CCM ones, the maximum error reaching 17.2%.

Eventually, it is worth observing that, although the absolute values of the finite crack extension and the process zone do not match each other, their trend with respect to the notch opening angle (see Fig. 5b) is the same. The finite crack advance Δ_c increases monotonically from the value $(1/2\pi) \times l_{ch}$, i.e. the critical distance according to PM, to the limit value $2/(1.12^2\pi) \times l_{ch} = 0.506 \times l_{ch}$, i.e. the critical distance for the LE approach for edge cracks [13]. Although this latter value does not coincide with the one for a vanishing central crack (see Section 2), a good correspondence between the finite crack advancement ahead a crack of length a and ahead a deep V-notch with opening angle $\omega = 2 \arctan(l_{ch}/a)$ is observed, see Fig. 6a.

4. Conclusions

In recent years, several contributions in the Scientific Literature have proven the soundness of FFM by means of a comparison with experimental data (see e.g. [26–30]). On the other hand, in the present paper we corroborated the FFM approach by showing that failure load estimates are very close to the ones provided by the widely-spread CCM for a couple of case studies: short cracks and V-notches. Noteworthy, by exploiting shape functions available in the Scientific Literature, the solutions for both models are provided analytically.

The comparison was carried out by assuming a rectangular cohesive law (i.e. of Dugdale-type) for the CCM and a pointwise stress condition for the FFM criterion, this choice being at the same time the simplest one, leading to analytical results, and the most reasonable one. Resting on a linear elastic solution, FFM is much easier to apply with respect to the CCM. Thus, the small differences between the CCM and FFM predictions (few unit percent for the geometries analyzed) corroborate the use of FFM as an effective tool for preliminary sizing and optimization of structural components.

Appendix A

Eq. (11) was derived and solved originally by Cornetti et al. [31]. Introducing the following quantity:

$$f = \sqrt[3]{1 + \frac{\pi}{4}\frac{a}{l_{ch}}\left[-6 + \frac{\pi}{2}\frac{a}{l_{ch}}\left(15 + 8\pi\frac{a}{l_{ch}}\right) + 3\sqrt{\frac{\pi}{2}\frac{a}{l_{ch}}\left(12 - 39\frac{\pi}{2}\frac{a}{l_{ch}} + 24\pi^2\frac{a^2}{l_{ch}^2}\right)}\right]} \tag{A1}$$

the real solution of the cubic Eq. (11) providing the discrete crack advancement becomes:

$$\frac{\Delta_c}{l_{ch}} = \frac{2}{3\pi f}\left[f^2 + \left(1 - 2\pi\frac{a}{l_{ch}}\right)f + \left(1 - \pi\frac{a}{l_{ch}} + \pi^2\frac{a^2}{l_{ch}^2}\right)\right] \tag{A2}$$

Appendix B

The shape function β in Eq. (19) is most conveniently expressed vs. $\alpha = \pi - \omega/2$ (see Fig. 4a). Its (exact) expression reads [25]:

$$\beta = \sqrt{\frac{2\alpha + \sin(2\alpha)}{\alpha^2 + \sin^2\alpha}} \tag{B1}$$

Introducing the quantity $c = \pi\beta^2/2$, the approximate expression for μ in Eq. (15) provided by Savruk and Rytsar [23] reads:

$$\mu = \frac{(2\pi)^\lambda}{\pi\sqrt{2c}}\frac{\Gamma\left(\frac{\lambda}{c}\right)}{\Gamma\left(\frac{\lambda}{c} + \frac{1}{2}\right)} \tag{B2}$$

where Γ is the Gamma function.

Eventually, the approximate expression for γ in Eq. (16) proposed by Tada et al. [12] is equal to:

$$= \sqrt{\pi}\frac{0.1755 + 0.219(\alpha/\pi) + 0.385(\alpha/\pi)^2 + 0.120(\alpha/\pi)^3}{(\alpha/\pi)^{1.5}} \tag{B3}$$

References

[1] Cornetti P, Pugno N, Carpinteri A, Taylor D. Finite fracture mechanics: a coupled stress and energy failure criterion. Engng Fract Mech 2006;73:2021–33.
[2] Camanho PP, Erçin GH, Catalanotti G, Mahdi S, Linde P. A finite fracture mechanics model for the prediction of the open-hole strength of composite laminates. Composites Part A 2012;43:1219–25.

[3] Leguillon D. Strength or toughness? A criterion for crack onset at a notch. Eur J Mech A/Solids 2002;21:61–72.
[4] Mantič V. Interface crack onset at a circular cylindrical inclusion under a remote transverse tension. Application of a coupled stress and energy criterion. Int J Solids Struct 2009;46:1287–304.
[5] Wang JT. Investigating some technical issues on cohesive zone modeling of fracture. J Eng Mater Technol-Trans ASME 2013;135(1) 011003.
[6] Carpinteri A, Cornetti P, Pugno N, Sapora A, Taylor D. A finite fracture mechanics approach to structures with sharp V-notches. Engng Fract Mech 2008;75:1736–52.
[7] Cornetti P, Mantič V, Carpinteri A. Finite fracture mechanics at elastic interfaces. Int J Solids Struct 2012;49:1022–32.
[8] Bažant ZP, Li YN. Stability of cohesive crack model: Part II—Eigenvalue analysis of size effect on strength and ductility of structures. J Appl Mech – ASME 1995;62:965–9.
[9] Bertram Broberg K. Cracks and fracture. London: Academic Press; 1999.
[10] Carpinteri A, Cornetti P, Pugno N, Sapora A. The problem of the critical angle for edge and center V-notched structures. Eur J Mech A/Solids 2011;30:281–5.
[11] Dugdale DS. Yielding of steel sheets containing slits. J Mech Phys Solids 1960;8:100–8.
[12] Tada H, Paris P, Irwin G. The stress analysis of cracks. Handbook. St Louis: Paris Production Incorporated; 1985.
[13] Taylor D, Cornetti P, Pugno N. The fracture mechanics of finite crack extension. Engng Fract Mech 2005;72:1021–38.
[14] Carpinteri A. Stress-singularity and generalized fracture toughness at the vertex of re-entrant corners. Engng Fract Mech 1987;26:143–55.
[15] Hills DA, Dini D. Characteristics of the process zone at sharp notch roots. Int J Solids Struct 2011;48:2177–83.
[16] Flicek RC, Hills DA, Dini D. Refinements in the characterisation of mode-mixity and small scale yielding at sharp notch roots. Engng Fract Mech 2014;126:73–86.
[17] Gomez FJ, Elices M. Fracture of components with V-shaped notches. Engng Fract Mech 2003;70:1913–27.
[18] Henninger C, Leguillon D, Martin E. Crack initiation at a V-notch – comparison between a brittle fracture criterion and the Dugdale cohesive model. Comptes Rendu Mécanique 2007;335:388–93.
[19] Shi WC. Equivalence of the notch stress intensity factor, tip opening displacement and energy release rate for a sharp V-notch. Int J Solids Struct 2014;51:904–9.
[20] Hasebe N, Iida J. A crack originating from a triangular notch on a rim of a semi-infinite plate. Engng Fract Mech 1978;10:773–82.
[21] Philipps AG, Karuppanan S, Churchman CM, Hills DA. Crack tip stress intensity factors for a crack emanating from a sharp notch. Engng Fract Mech 2008;75:5134–9.
[22] Livieri P, Tovo R. The use of the JV parameter in welded joints: stress analysis and fatigue assessment. Int J Fatigue 2009;31:153–63.
[23] Savruk MP, Rytsar PB. A closed approximate solution of a plane problem of the theory of elasticity for a wedge with symmetric crack. In: Panasyuk VV, editor. Fracture mechanics of materials and strength of structures [in Ukrainian], vol. 2, Kamenyar, Lviv; 1999, p. 125–8.
[24] Kazberuk A. Stress intensity factors for cracks at the vertex of a rounded V-notch. Mater Sci 2009;45:676–87.
[25] Ouchterlony F. Symmetric cracking of wedge by concentrated loads. Int J Engng Sci 1977;15:109–16.
[26] Yosibash Z, Priel E, Leguillon D. A failure criterion for brittle elastic materials under mixed-mode loading. Int J Fract 2006;141:291–312.
[27] Hebel J, Dieringer R, Becker W. Modelling brittle crack formation at geometrical and material discontinuities using a finite fracture mechanics approach. Engng Fract Mech 2010;77:3558–72.
[28] Andersons J, Tarasovs S, Sparniņš E. Finite fracture mechanics analysis of crack onset at a stress concentration in a UD glass/epoxy composite in off-axis tension. Compos Sci Technol 2010;70:1380–5.
[29] Weißgraeber P, Becker W. Finite fracture mechanics model for mixed mode fracture in adhesive joints. Int J Solids Struct 2013;50:2383–94.
[30] Cornetti P, Sapora A, Carpinteri A. T-stress effects on crack kinking in finite fracture mechanics. Engng Fract Mech 2014;132:169–76.
[31] Cornetti P, Sapora A, Carpinteri A. Finite fracture mechanics vs. cohesive crack modelling: an analytical comparison based on case studies. In: 16th European conference on composite materials, 22–26 June, Seville, Spain; 2014.